Article

Towards Zn-dominant Tourmaline: a Case of Zn-rich Fluor-Elbaite and Elbaite from the Julianna System at Piława Górna, Lower Silesia, SW Poland

Adam Pieczka [1,*], Bożena Gołębiowska [1], Piotr Jeleń [2], Adam Włodek [1], Eligiusz Szełęg [3] and Adam Szuszkiewicz [4]

[1] AGH University of Science and Technology, Department of Mineralogy, Petrography and Geochemistry, 30-059 Kraków, Mickiewicza 30, Poland; goleb@agh.edu.pl (B.G.); wlodek@agh.edu.pl (A.W.)
[2] AGH University of Science and Technology, Faculty of Materials Science and Ceramics, 30-059 Kraków, Mickiewicza 30, Poland; pjelen@agh.edu.pl
[3] University of Silesia in Katowice, Faculty of Earth Sciences, 41-200 Sosnowiec, Będzińska 60, Poland; eligiusz.szeleg@us.edu.pl
[4] University of Wrocław, Institute of Geological Sciences, 50-204 Wrocław, pl. M. Borna 9, Poland; adam.szuszkiewicz@uwr.edu.pl
* Correspondence: pieczka@agh.edu.pl; Tel.: +48-12-6172144

Abstract: Tourmalines are a group of minerals which may concentrate various accessory components, e.g. Cu, Ni, Zn, Bi, Ti, Sn. The paper presents fluor-elbaite and elbaite from a dyke of the Julianna pegmatitic system at Piława Górna, at the NE margin of the Bohemian Massif, SW Poland, containing up to 6.32 and 7.37 wt.% ZnO, respectively. Such high amounts of ZnO are almost two times higher than in the second most Zn-enriched tourmaline known to date. The compositions of the Zn-rich tourmalines from Piława Górna, studied by electron microprobe and Raman spectroscopy, correspond to the formulae: $(Na_{0.73}Ca_{0.01}\square_{0.25})_{\Sigma 1}(Al_{1.03}Li_{0.79}Zn_{0.76}Fe^{2+}_{0.33}Mn_{0.09})_{\Sigma 3}Al_6B_3Si_6O_{27}(OH)_3(F_{0.66}OH_{0.34})$, and $(Na_{0.78}Ca_{0.01}\square_{0.21})_{\Sigma 1}(Al_{1.06}Li_{0.87}Zn_{0.88}Fe^{2+}_{0.10}Mn_{0.09})_{\Sigma 3}Al_6B_3Si_6O_{27}(OH)_3(OH_{0.84}F_{0.16})$, respectively, with Zn as one of the main octahedral occupants. A comparison with other tourmalines and associated Zn-rich fluor-elbaite and elbaite from the pegmatite indicates that atypically high Zn-enrichment is not a result of Zn-Fe fractionation, but dissolution and reprecipitation induced by a late (Na,Li,B,F)-bearing fluid within the assemblage of gahnite spinel and primary schorl-type tourmaline. This strongly suggests Na-Li-B-F metasomatism of gahnite-bearing mineral assemblages as that is the only environment that can promote crystallization of a hypothetical Zn-dominant tourmaline. The compositions of the Zn-rich fluor-elbaite and elbaite suggest three possible end-members for such a hypothetical tourmaline species: $NaZn_3Al_6B_3Si_6O_{27}(OH)_3(OH)$, $\square(Zn_2Al)Al_6B_3Si_6O_{27}(OH)_3(OH)$ and $Na(Zn_2Al)Al_6B_3Si_6O_{27}(OH)_3O$.

Keywords: tourmaline, fluor-elbaite, elbaite, Zn-enrichment, electron microprobe, Raman spectroscopy, granitic pegmatites, Piława Górna, Sudetes

1. Introduction

Tourmalines are a supergroup of accessory minerals, common in various igneous, metamorphic and sedimentary rocks. They are complex borosilicates with the generalized chemical formula $XY_3Z_6(T_6O_{18})(BO_3)_3V_3W$ [1], where X, Y, Z, T, B, V (=O3) and W (=O1) denote structural sites occupied by:

X – Na^+, K^+, Ca^{2+}, Pb^{2+}, $\square$ (vacancy),
Y – Fe^{2+}, Mg^{2+} , Mn^{2+}, Al^{3+}, Li^+, Fe^{3+}, Cr^{3+}, V^{3+}, Ti^{4+}, Zn^{2+}, Cu^{2+}, Ni^{2+}, …
Z – Al3+, Fe3+, Cr3+, V3+, Mg2+, Fe2+, ...
T – Si^{4+}, Al^{3+}, B^{3+},
B – B^{3+};
V – OH^-, O^{2-},

W – OH^-, F^-, O^{2-}.

The extremely complex chemical composition results in a number of minerals accepted as valid species by the Commission on New Minerals, Nomenclature and Classification of the International Mineralogical Association (IMA CNMNC), or reported but not IMA-approved, e.g. an unnamed Pb-dominant tourmaline (up to 17.5 wt.% PbO; [2]). Varieties atypically enriched in other elements, which do not attain the status of the dominant component in any structural site in any tourmaline species, are also occasionally found. For example, apart from the relatively common (Fe^{2+}, Mg^{2+}, Mn^{2+}, Al^{3+}, Al^{3+}+Li^+, Fe^{3+}, Cr^{3+} or V^{3+})-dominant tourmalines, there are also known crystals enriched in Ti^{4+} (up to 4.07 wt.% TiO_2; [3]), Sn^{4+} (up to 0.42 wt.% Sn; [4]), Bi^{3+} (up to 0.49 wt.% Bi_2O_3; [5]), Cu^{2+} (up to 3.51 wt.% CuO; [6]), Ni^{2+} (up to 3.96 wt.% NiO; [7]), and Zn^{2+}. Other admixtures may also be present although do not attain such spectacular concentrations.

Zinc is found in numerous tourmalines, although commonly at amounts not exceeding a few tenths of wt.%. Rare findings of tourmalines with ZnO > 1 wt.% have been reported, for instance, from Cross Lake, Manitoba, Canada (1.24 wt.%; [8]), Minas Gerais (1.72 wt.%; [9]; 1.88 wt.%; [10]) and Rio Grande do Norte (2.15 wt.%; [11]; 2.43 wt.%; [12]; 3.01 wt.%; [13]) in Brazil, and from Congo (2.85 wt.%; [14]). The most Zn-enriched tourmaline (3.83 wt.% ZnO) has been described from Russia [15].

In this paper, we describe fluor-elbaite and elbaite with almost 7.5 wt.% ZnO from the Julianna system of anatectic pegmatites at Piława Górna, Góry Sowie Block, SW Poland. We discuss their chemistry, propose possible explanations for such high Zn enrichment and suggest the most probable environments for formation of even more Zn-rich crystals.

2. Geological setting

Zinc-enriched tourmaline was found in a pegmatite of the Julianna pegmatitic system exposed in an amphibolite-migmatite quarry (50º42'11.77''N, 16º44'12.36''E) near Piława Górna, ~50 km southwest of Wrocław, SW Poland (Fig. 1). The quarry is located in the Góry Sowie Block (GSB), a tectono-stratigraphic unit that is mostly built of a polymetamorphic metasedimentary-metavolcanic sequence and is situated at the north-eastern periphery of the Bohemian Massif in the European Variscides. The Julianna system is composed of coeval and cogenetic dykes, apophyses and lenticular bodies, up to 6–7 m thick, extending along 30–40 m in vertical section, 80–100 m in planar view along a NNE–SSW running zone of strongly tectonized amphibolite [16]. The pegmatites show a broad range of textural differentiation from homogeneous and subhomogeneous to simply zoned bodies (border zone + wall zone + graphic intermediate zone + blocky-feldspar intermediate zone + quartz core ± quartz-albite zone ± spodumene–'lepidolite' core). Geochemical variability varies from primitive and moderately fractionated pegmatites, enriched in Nb-REE-Be-B and belonging to the NYF (niobium-yttrium-fluorine) pegmatitic family, to rare and much more strongly fractionated pods located in the axial parts of the largest dykes that contain Li-Cs-Ta-Be-B mineralization of the LCT (lithium-cesium-tantalum) type [16–19]. The pegmatites are formed mainly of microcline, Na-plagioclase, quartz, 'biotite' and muscovite, accompanied by schorl, almandine-spessartine garnet and beryl. Rare-element mineralization of the prevalent NYF-affiliated pegmatites includes, among others, columbite-group minerals, ixiolite, ferrowodginite, samarskite-, euxenite- and fergusonite-group minerals, pyrochlore-supergroup minerals, cassiterite, ilmenite and titanite, gadolinite-group minerals, hellandite-(Y), keiviite-(Y), pilawite-(Y), allanite-group minerals, xenotime-(Y), and monazite-(Ce). Highly fractionated pods with the LCT-type mineralization contain, among others, 'zinnwaldite', 'lepidolite', a Cs-bearing dark mica, spodumene, pollucite, cassiterite, spessartine, tantalite-(Mn), minerals of the microlite group, elbaite–liddicoatite–rossmanite tourmaline, Cs-bearing beryl and pezzottaite. Mineralogy and petrography of the Julianna pegmatites have been systematically studied [16, 18, 20–22] and the occurrence is the type locality for pilawite-(Y), bohseite and żabińskiite [23–25].

Dating of Julianna pegmatites gave an emplacement age of 377.6 ± 1.3 Ma [U-Th-Pb; monazite-(Ce)] and 380.7 ± 2.4 Ma (U-Pb-Th; uraninite) [19, 26]. These ages point to their formation by the anatectic melting of the metasedimentary-metavolcanic GSB rocks during tectonic

exhumation at 385-370 Ma [27–29]. Recent studies of trace elements in quartz from the Julianna pegmatites and their host rocks comply with this model and suggest that the pegmatite-forming melt was most probably generated at pressures ~5 kbar, at a slightly greater depth than the present day exposure level [30]. The geochemical diversity of the metasedimentary-metavolcanic protolith, similar to paragneisses and amphibolites exposed in the Piława Górna quarry, is a plausible source for highly enriched partial melts with hybrid NYF + LCT characteristics.

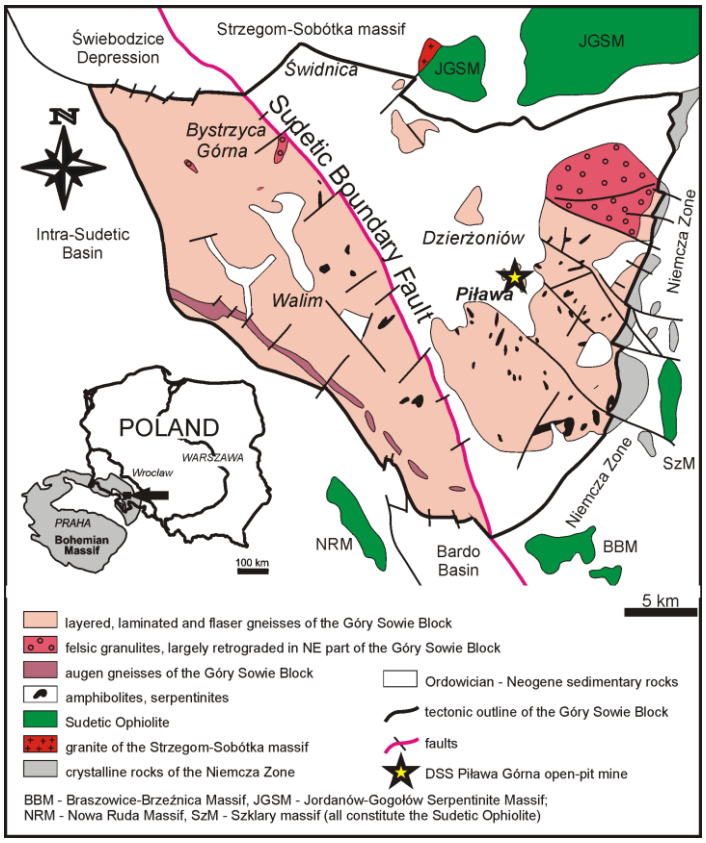

Figure 1. Simplified geological map of the Góry Sowie Block with the location of the Piława Górna quarry (after Szuszkiewicz *et al*. [16]).

3. Occurrence

The pegmatite dyke with the Zn-rich tourmaline was exposed in the Piława quarry in 2010, when it could be observed along a few tens of meters in horizontal section with a maximum thickness of ~3–4 m. The dyke showed typical zoning, and the assemblage of accessory minerals position it as transitional between NYF- and LCT-type pegmatites. Fan-shaped aggregates of muscovite, a few centimeters in length, in the graphic zone are a characteristic feature of this pegmatite. Short prismatic crystals of light-grey-bluish beryl, up to 5 cm long, occur together with quartz in interstices among feldspar crystals in the blocky feldspar zone and in the quartz core [18]. The blocky feldspar zone and the quartz core contain also up to 7 cm long intergrowths and radial aggregates of black tourmaline, up to 4–5 cm large quartz–garnet (almandine–spessartine series) symplectitic intergrowths, a few centimeter sized books of pale greenish muscovite, relatively abundant cassiterite (up to 3 cm large) and columbite-group minerals (up to 4 cm in length), as well as subordinate a few millimeter sized dark greenish crystals of gahnite. Lithium-bearing tourmalines were found only occasionally in the form of small, up to 2 cm long, dark green crystals within the books of greenish K-mica. Electron microprobe studies of the collected material reveal also the presence of columbite-(Fe) and columbite-(Mn), ferrowodginite and wodginite, various pyrochlore-supergroup minerals (fluor-calciomicrolite, hydroxyl-calciomicrolite or keno-calciomicrolite, hydroxyl-plumbomicrolite or oxy-plumbomicrolite, hydromicrolite and hydropyrochlore grading to zero-valence-dominant microlite and pyrochlore, and

fluor-calcioroméite), a Fe-bearing Cs-dominant dark mica, genthelvite, uraninite, monazite-(Ce), xenotime-(Y), cheralite, zircon, scheelite, sphalerite, ferronigerite and zinconigerite, lithiophilite, alluaudite, hydroxylapatite, mitridatite and other unrecognized phosphates, pucherite, and probably also cookeite and chamosite. Zinc-rich tourmaline was found only along the contact between adjacent gahnite and primary schorl-type tourmaline evolving to secondary fluor-elbaite.

4. Methods

4.1. Electron microprobe analysis (EMPA)

Electron microprobe analyses of tourmalines were performed at the Inter-Institute Analytical Complex for Minerals and Synthetic Substances at the University of Warsaw, Poland, using a Cameca SX 100 electron microprobe operating in wavelength-dispersive mode under the following conditions: accelerating voltage of 15 kV, beam current of 10 nA, beam diameter of 2 μm, peak count-time of 20 s, background time of 10 s. Standards, diffracting crystals, analytical lines and mean detection limits (in wt.%) were as follows: fluorophlogopite – F (PC0, *Kα*, 0.12), albite – Na (TAP, *Kα*, 0.03), diopside – Mg (TAP, *Kα*, 0.02), Si (TAP, *Kα*, 0.03) and Ca (PET, *Kα*, 0.02), orthoclase – Al (TAP, *Kα*, 0.03) and K (PET, *Kα*, 0.02), rutile – Ti (LPET, *Kα*, 0.02), rhodonite – Mn (LIF, *Kα*, 0.09), hematite – Fe (LIF, *Kα*, 0.08), V2O5 – V (LIF, *Kα*, 0.06), Cr2O3 – Cr (LPET, *Kα*, 0.02), and sphalerite – Zn (LIF, *Kα*, 0.09). The raw data were reduced with the PAP routine of Pouchou and Pichoir [31].

Atomic contents were normalized to 15 Y + Z + T atoms per formula unit (*apfu*) for schorl-type tourmalines with Y + Z > 9 *apfu* ($Li_{calc.}$ = 0 *apfu*), and on the basis of 6 Si *apfu* for Li-bearing tourmalines, with B_2O_3 calculated with the assumption of 3 B *apfu*, Li = 9 – $(Y + Z)_{EMPA}$ *apfu*, where $(Y + Z)_{EMPA}$ denotes the total of all octahedral Y- and Z-site occupants determined by EMPA, Fe_{total} = Fe^{2+}, and H_2O occurring as OH groups by stoichiometry based on electroneutrality of the formulae. For analyses showing OH + F > 4 *apfu* due to excesses of microprobe determined SiO_2 (quartz nanoinclusions), the amount of the component was reduced to a value for which the stoichiometric OH + F = 4 *apfu* was achieved, i.e. the highest content accepted for the tourmaline structure.

4.2. Raman spectroscopy

Raman spectra were collected in back-scattered geometry at the Faculty of Materials Science and Ceramics, AGH UST, Cracow, Poland, with a Horiba Labram HR spectrometer integrated with an Olympus BX 40 confocal microscope equipped with a Nd: YAG, 532 nm (10mW) laser and 1800 gr/mm grating. The spectra were recorded in the range 4000–50 cm^{-1} on randomly oriented surfaces of crystals mounted in epoxy resin in a 1-inch disc that was used also for EMPA studies. The Raman measurements were carried out with an estimated analytical spot size of ~1 μm, the microscope magnification 100×, an acquisition time of 600 s and accumulation of 2 scans. Calibration was done using the 520.7 cm^{-1} line of Si.

5. Results

5.1. Primary tourmalines

The only tourmalines discernible by naked eye in hand specimens are a few centimetres large, black, and sometimes radially intergrown crystals of primary schorl (Trm I). The crystals display almost constant FeO contents [13.27(30)–12.66(29) wt.%; 1.88(4)–1.81(4) Fe *apfu* on average] and small Si deficiency [5.97(2) and 5.94(3) Si *apfu*, respectively] (Table 1). However, they show some heterogeneity in other chemical components as well as some Mn-Fe fractionation. The most primitive variety is Trm IA, with Mn/(Mn+Fe) = 0.010(2), and depletion in Al [6.14(6) *apfu* on average]. More evolved is Trm IB that shows Mn/(Mn+Fe) = 0.029(14)–0.034(4), and much higher Al content of 6.79(11)–6.91(4) *apfu*. Compared to Trm IB, Trm IA is also enriched in Na [0.66(3) *vs*.

Table 1. Average compositions of primary schorl-type tourmaline.

wt.%	Trm IA	Trm IB	
SiO_2	35.21(0.25)	35.11(0.27)	34.84(0.28)
TiO_2	1.11(0.30)	0.09(0.03)	0.10(0.03)
$B_2O_{3(calc.)}$	10.25(0.06)	10.26(0.04)	10.19(0.06)
Al_2O_3	30.86(0.38)	34.28(48)	34.38(0.32)
FeO	13.27(0.30)	13.04(0.31)	12.66(0.29)
MnO	0.14(0.03)	0.39(0.18)	0.45(0.06)
MgO	3.19(0.23)	1.03(0.43)	0.89(0.18)
ZnO	0.07(0.06)	0.30(0.10)	0.27(0.04)
CaO	0.48(0.10)	0.06(0.06)	0.03(0.02)
$Li_2O_{(calc.)}$			
Na_2O	2.01(0.10)	1.77(0.10)	1.64(0.14)
K_2O	0.04(0.02)	0.03(0.01)	0.04(0.01)
H_2O	3.25(0.06)	3.16(0.11)	3.07(0.05)
F_2	0.14(0.07)	0.14(0.08)	0.23(0.03)
-O=F2	-0.06(0.03)	-0.06(0.04)	-0.10(0.01)
Total	99.96(56)	99.60(0.44)	98.68(0.59)
apfu			
$^{X}Na^{+}$	0.66(0.03)	0.58(0.03)	0.54(0.05)
$^{X}K^{+}$	0.01(0.00)	0.01(0.00)	0.01(0.00)
$^{X}Ca^{2+}$	0.09(0.02)	0.01(0.01)	0.01(0.00)
$^{X}\square$	0.24(0.04)	0.40(0.04)	0.44(0.05)
ΣX	1.00	1.00	1.00
Mg^{2+}	0.81(0.06)	0.26(0.11)	0.23(0.05)
Fe^{2+}	1.88(0.04)	1.85(0.04)	1.81(0.04)
Mn^{2+}	0.02(0.00)	0.06(0.03)	0.06(0.01)
Zn^{2+}	0.01(0.00)	0.04(0.01)	0.03(0.01)
Al^{3+}	6.14(0.06)	6.79(0.11)	6.85(0.04)
Ti^{4+}	0.14(0.04)	0.01(0.00)	0.01(0.00)
$\Sigma(Y+Z)$	9.00	9.00	9.00
$^{B}B^{3+}$	3.00	3.00	3.00
$^{T}Si^{4+}$	5.97(0.02)	5.95(0.04)	5.94(3)
$^{T}Al^{3+}$	0.03(0.02)	0.05(0.04)	0.06(3)
ΣT	6.00	6.00	6.00
O	27.00	27.00	27.00
$^{V}OH^{-}$	3.00	3.00	3.00
$^{W}O^{2-}$	0.24(0.05)	0.36(0.09)	0.39(0.05)
$^{W}OH^{-}$	0.68(0.06)	0.56(0.12)	0.49(0.05)
$^{W}F^{-}$	0.08(0.03)	0.07(0.04)	0.12(0.02)
ΣW	1.00	1.00	1.00
Mn#	0.010(0.002)	0.029(0.014)	0.034(0.004)

Mn# = Mn/(Mn+Fe).

0.58(3)–0.54(5) *apfu*] and Mg [0.81(6) *vs*. 0.26(11)–0.23(5) *apfu*], and shows higher contents of such trace components as Ca [0.09(2) *vs*. 0.01(0.01) *apfu*] and Ti [0.14(4) *vs*. 0.01(0) *apfu*], and lower amounts of Mn [0.02(<1) *vs*. 0.06(3) *apfu*] and Zn [0.01(0) *vs*. 0.03(1)–0.04(1) *apfu*]. Fluorine contents are almost the same in Trm IA and Trm IB [0.08(3) *vs*. 0.07(4)–0.12(2) *apfu*, respectively] and the *W* site in both types of schorl is dominated by monovalent anions (OH^{-} + F^{-}) with OH^{-} > F^{-}, with slightly increasing $^{W}O^{2-}$ in the more evolved variety [0.24(5) *vs*. 0.36(9)–0.39(5) *apfu* in Trm IA and Trm IB, respectively].

5.2. Secondary dark bluish Li-bearing tourmaline in quartz

Table 2. Representative compositions of dark bluish (Trm IIA) and dark green (Trm IIB) tourmaline.

	dark bluish inclusions in quartz					dark green crystals in muscovite				
wt.%	223/9	217/3	217/4	217/6	217/5	112/28	112/23	112/16	112/17	112/20
SiO_2	36.36	35.68	37.00	36.77	36.73	36.25	36.64	37.03	37.13	37.45
TiO_2	0.03	0.15	0.07	0.07	0.02	0.19	0.07	0.08	0.08	0.08
$B_2O_{3(calc.)}$	10.53	10.34	10.72	10.65	10.64	10.50	10.61	10.73	10.76	10.85
Al_2O_3	35.14	35.47	36.12	36.71	36.64	36.60	37.79	37.97	38.09	38.74
FeO	10.96	9.95	8.64	5.44	5.52	8.24	7.49	6.53	5.67	5.10
MnO	1.24	0.69	0.73	0.90	0.99	0.73	0.69	0.85	0.82	0.97
MgO	0.05	0.07	0.08	0.03	0.02	0.13	0.13	0.10	0.11	0.13
ZnO	0.49	0.56	0.49	1.03	1.17	0.17	0.13	0.38	0.93	0.57
CaO	0.03	0.12	0.18	0.17	0.15	0.60	0.07	0.10	0.12	0.15
$Li_2O_{(calc.)}$	0.61	0.54	1.14	1.43	1.38	0.82	0.80	1.03	1.11	1.18
Na_2O	1.74	2.17	2.38	2.54	2.51	2.28	2.35	2.52	2.41	2.47
K_2O	0.02	0.04	0.05	0.02	0.00	0.03	0.02	0.00	0.03	0.00
$H_2O_{(calc.)}$	3.49	2.87	3.32	3.28	3.08	2.74	2.80	2.82	2.89	2.95
F_2	0.27	0.61	0.80	0.83	1.25	0.73	0.75	1.03	1.05	0.90
$-O=F_2$	-0.12	-0.26	-0.34	-0.35	-0.53	-0.31	-0.32	-0.43	-0.44	-0.38
Total	100.85	99.00	101.37	99.53	99.58	99.69	100.04	100.73	100.74	101.15
apfu										
$^{X}Na^{+}$	0.56	0.71	0.75	0.80	0.80	0.73	0.75	0.79	0.75	0.77
$^{X}K^{+}$	0.00	0.01	0.01	0.01	0.00	0.01	0.00	0.00	0.01	0.00
$^{X}Ca^{2+}$	0.01	0.02	0.03	0.03	0.03	0.11	0.01	0.02	0.02	0.03
$^{X}\square$	0.43	0.26	0.21	0.16	0.16	0.16	0.24	0.19	0.22	0.21
ΣX	1.00	1.00	1.00	1.00	1.00	1.00	1.00	1.00	1.00	1.00
Li^{+}	0.40	0.36	0.74	0.94	0.91	0.54	0.53	0.67	0.72	0.76
Mg^{2+}	0.01	0.02	0.02	0.00	0.01	0.03	0.03	0.02	0.03	0.03
Fe^{2+}	1.51	1.40	1.17	0.74	0.75	1.14	1.03	0.88	0.77	0.68
Mn^{2+}	0.17	0.10	0.10	0.12	0.14	0.10	0.10	0.12	0.11	0.13
Zn^{2+}	0.06	0.07	0.06	0.12	0.14	0.02	0.02	0.05	0.11	0.07
Al^{3+}	6.83	7.03	6.90	7.06	7.05	7.14	7.29	7.25	7.25	7.32
Ti^{4+}	0.01	0.02	0.01	0.01	0.00	0.02	0.01	0.01	0.01	0.01
$\Sigma(Y+Z)$	9.00	9.00	9.00	9.00	9.00	9.00	9.00	9.00	9.00	9.00
$^{B}B^{3+}$	3.00	3.00	3.00	3.00	3.00	3.00	3.00	3.00	3.00	3.00
$^{T}Si^{4+}$	6.00	6.00	6.00	6.00	6.00	6.00	6.00	6.00	6.00	6.00
O	27.00	27.00	27.00	27.00	27.00	27.00	27.00	27.00	27.00	27.00
$^{V}OH^{-}$	3.00	3.00	3.00	3.00	3.00	3.00	3.00	3.00	3.00	3.00
$^{W}O^{2-}$	0.01	0.46	0.00	0.00	0.00	0.59	0.56	0.43	0.35	0.39
$^{W}OH^{-}$	0.85	0.21	0.59	0.57	0.36	0.02	0.05	0.04	0.11	0.15
$^{W}F^{-}$	0.14	0.32	0.41	0.43	0.64	0.38	0.39	0.53	0.54	0.46
ΣW	1.00	1.00	1.00	1.00	1.00	1.00	1.00	1.00	1.00	1.00
Mn#	0.103	0.066	0.079	0.143	0.154	0.082	0.086	0.116	0.127	0.161
	Sch	F-sch	Elb	Elb	F-elb	Dh	Dh	F-elb	F-elb	F-elb

Mn# = Mn/(Mn+Fe). Abbreviations: Sch – schorl, F-sch – fluor-schorl, Elb – elbaite, Dh – darrelhenryite, F-elb – fluor-elbaite.

Anhedral inclusions (< 1mm) of dark bluish Li-bearing tourmaline (Trm IIA) in quartz, replacing schorl and fluor-schorl, are discernible under a stereomicroscope or in back-scattered-electron (BSE) images. The schorl-type primary tourmaline is slightly enriched in Li_2O (up to ~0.61 wt.%; ~0.40 Li apfu) (Table 2). However, low contents of Ca (0.01–0.02 *apfu*) and Ti (0.00–0.02 *apfu*), depletion in Fe down to 1.51–1.40 *apfu*, enrichment in Al (6.83–7.03 *apfu*), Mn (0.10–0.17 *apfu*) and Zn (0.06–0.07 *apfu*; 0.49–0.56 wt.% ZnO), as well as the degree of Mn-Fe

fractionation [Mn/(Mn+Fe) = 0.060–0.103] indicate that it corresponds to the primary Al-bearing Trm IB. The $^{W}O^{2-}$ content in this tourmaline reaches 0.46 *apfu*.

Secondary Trm IIA represents elbaite and fluor-elbaite with rather constant Na (0.72–0.80 *apfu*). Compared to its Trm IB precursor, it has generally higher, though partly overlapping Mn/(Mn+Fe) ratio of 0.080–0.183, similar or slightly higher contents of Al (up to 7.07 *apfu*) and Mn (0.09–0.17 *apfu*), a noticeable increase of Zn (0.06–0.14 *apfu*; up to 1.17 wt.% ZnO), decrease of Fe (down to 0.70 *apfu*) and constant low contents of Ca (~0.03 *apfu*), Mg (0.00–0.02 *apfu*) and Ti (0.00–0.01 *apfu*). Lithium can increase up to 0.94 *apfu*, and F up to 0.68 *apfu*.

5.3. Secondary dark greenish fluor-elbaite in muscovite books

Dark greenish translucent Li-tourmaline (Trm IIB) occurs as extremely rare, though relatively large, euhedral crystals up to 2 cm in length and 0.5 cm in diameter. In spite of the differences in color and size, the crystals are compositionally close to Trm IIA, except that the most Fe-enriched domains with 8.24–7.39 wt.% FeO (1.14–1.01 Fe *apfu*) are even more Al-enriched (up to 7.32 *apfu*) (Table 2). With increasing Mn-Fe fractionation [Mn/(Mn+Fe) = 0.082–0.161], the Trm IIB shows a decrease of Fe down to 0.68 *apfu*, coupled with an increase of Al and Mn up to 7.32 *apfu* and 0.13 *apfu*, respectively. Simultaneously, the calculated Li content increases from 0.53 *apfu* to 0.88 *apfu*. The amounts of Mg and Ti are negligible and usually close to 0.02–0.04 *apfu* and ~0.01 *apfu*, respectively. The contents of Zn vary randomly (0.13–0.93 wt.% ZnO; 0.02–0.11 Zn *apfu*), although generally increase in sectors with higher Mn-Fe fractionation degrees. With fluorine contents from 0.38 up to 0.59 *apfu* and $^{W}OH^{-} << WF^{-}$, Trm IIB classifies as fluor-elbaite. Only several Al-poorest and Fe-richest compositions, with lowest measured F and calculated Li contents and $^{W}O^{2-} > {}^{W}F^{-} + {}^{W}OH^{-}$, might be classified as Fe-bearing darrellhenryite [the end-member composition $Na(LiAl_2)Al_6B_3Si_6O_{27}(OH)_3O$].

5.4. Zn-rich tourmaline from gahnite dissolution – fluor-elbaite + elbaite reprecipitation zones

Zn-rich tourmaline (Trm III) was found as a secondary phase in a metasomatically altered assemblage of adjacent Trm IB (oxy-schorl to fluor-schorl) and gahnite. Highly-fractionated pale greenish gahnite with composition $Zn(Al_{1.98}Fe^{3+}_{0.02})O_4$ [Zn/(Zn+Fe) = 0.965(3)], typically occurs as fractured crystals, up to a few hundred micrometers in size, that are partly overgrown by Trm III (Fig. 2). Trm IB is usually largely dissolved and replaced by Trm IIIA (Zn-rich fluor-elbaite), forming clearly zoned crystals up to 1 millimeter in size (Fig. 2). Compositional maps (Fig. 3) present elemental distribution of Fe, Mn, Zn and Al in two areas, in which Zn-enriched tourmaline was detected. In both cases Fe concentration decreases gradually, coupled with increasing Zn and Al from the centre of the zoned crystals outwards (i.e. from Trm IB to Trm IIIA) and towards the adjacent gahnite. A local increase in Mn content in Trm IIIA is also marked. Trm IIIB (Zn-rich elbaite) occurs only as tiny domains, with the highest Zn concentration marked in Fig. 3 (Zn) as yellowish points within the greenish Zn-bearing matrix. The Zn-rich fluor-elbaite and elbaite appear only along the gahnite margins as a discontinuous zone with a maximum thickness of ~100 μm. Secondary Trm III contains sometimes relics of the primary tourmaline and numerous inclusions of mainly quartz and albite, sometimes gahnite, and very rarely sphalerite. Table 3 presents representative analyses of primary tourmaline and both secondary Zn-rich tourmalines. The chemical compositions of Trm IB in the gahnite-tourmaline assemblages do not differ from a typical composition of primary schorl Trm IB (Table 1). The Trm IIIA corresponds to fluor-elbaite with 0.54–0.66 *apfu* F and contains 7.00–7.05 *apfu* Al, 0.26–0.57 *apfu* Fe and 0.08–0.11 *apfu* Mn. The Trm IIIB, on the other hand, classifies as elbaite with 0.16–0.36 *apfu* F and has higher contents of Al (7.04–7.15 *apfu*), significantly lower concentrations of Fe (0.06–0.20 *apfu*) and similar amounts of Mn (0.05–0.10 *apfu*). Magnesium and Ti are below detection limits in both secondary tourmalines.

Preprints (www.preprints.org) | NOT PEER-REVIEWED | Posted: 18 January 2018 doi:10.20944/preprints201801.0176.v1

Peer-reviewed version available at Minerals 2018, 8, 126; doi:10.3390/min8040126

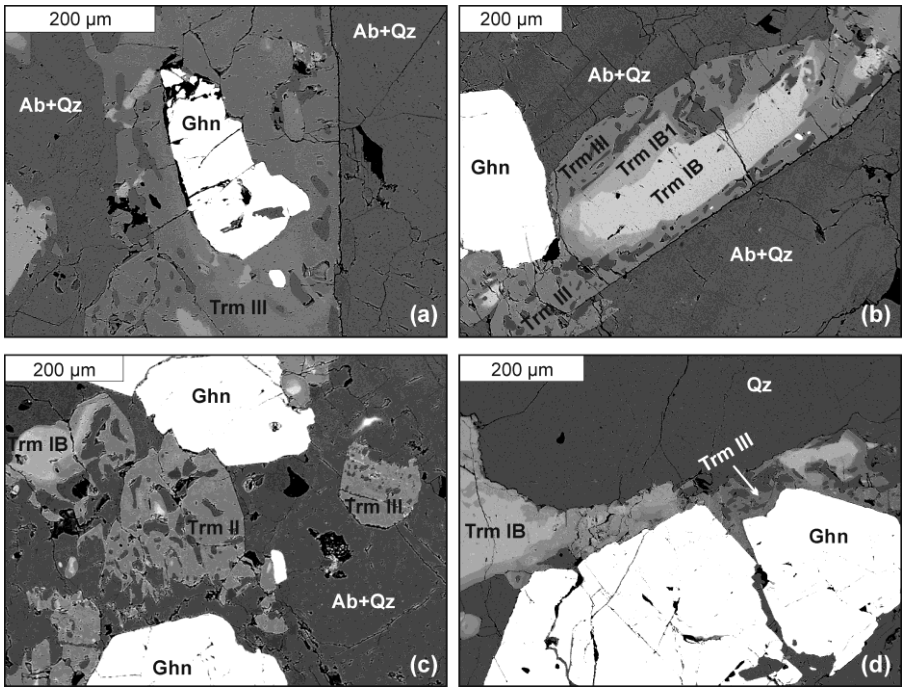

Figure 2. Back-scattered-electron images of Zn-rich tourmaline (Trm III) overgrowing primary schorl-type tourmaline IB and gahnite. Abbreviations: Ab – albite, Qz – quartz, Ghn – gahnite, Trm IB – primary, schorl-type tourmaline, Trm IB1 – fluor-schorl, Trm III – Zn-rich fluor-elbaite.

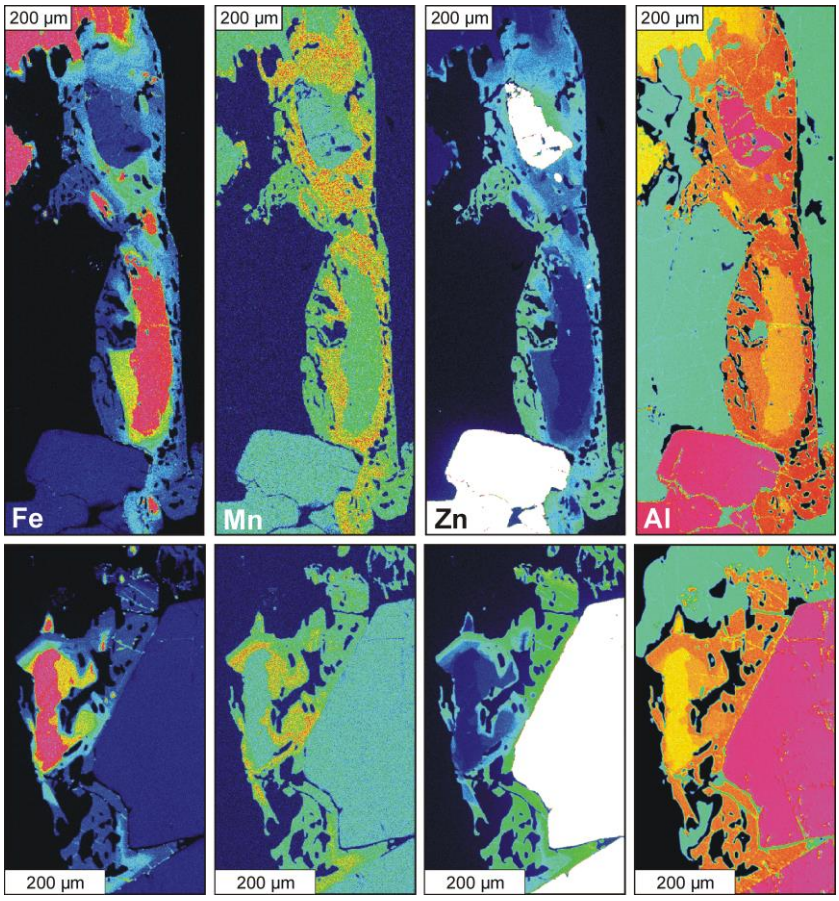

Figure 3. Fe-, Mn-, Zn- and Al-mapping for two occurrences of Zn-rich tourmaline (compare with Fig. 2). Color scale of increasing concentrations of the elements: dark blue–blue–green–yellow –orange–red–purple–white.

Table 3. Representative compositions of tourmalines of the Zn-rich assemblage.

	Trm IB	Trm IB1	Trm IIIA			Trm IIIB				
wt.%	1	2	3	4	5	6	7	8	9	10
SiO_2	34.96	35.83	36.73	37.08	36.97	37.05	36.61	37.25	36.79	37.11
TiO_2	0.18	0.06	0.03	0.00	0.00	0.00	0.00	0.00	0.00	0.00
$B_2O_{3(calc.)}$	10.13	10.38	10.64	10.74	10.71	10.73	10.61	10.79	10.66	10.75
Al_2O_3	33.57	35.08	36.48	36.98	36.72	37.17	36.86	37.67	36.99	37.05
FeO	13.27	9.76	3.21	1.92	1.89	1.26	1.17	0.62	0.51	0.71
MnO	0.82	1.06	0.72	0.76	0.63	0.52	0.60	0.48	0.54	0.69
MgO	0.18	0.06	0.00	0.00	0.00	0.00	0.00	0.00	0.00	0.00
ZnO	0.93	1.66	4.73	5.68	6.02	6.67	6.72	6.87	6.97	7.37
CaO	0.03	0.06	0.10	0.10	0.10	0.02	0.04	0.02	0.02	0.08
$Li_2O_{(calc.)}$	0.00	0.49	1.32	1.39	1.40	1.33	1.25	1.37	1.38	1.34
Na_2O	1.99	2.15	2.52	2.62	2.72	2.43	2.16	2.33	2.50	2.49
K_2O	0.03	0.00	0.00	0.00	0.00	0.00	0.02	0.00	0.00	0.00
$H_2O_{(calc.)}$	2.80	2.97	3.12	3.14	3.20	3.39	3.33	3.50	3.48	3.56
F_2	0.52	0.68	1.17	1.19	1.04	0.65	0.69	0.47	0.42	0.32
-O=F2	-0.22	-0.29	-0.49	-0.50	-0.44	-0.28	-0.29	-0.20	-0.18	-0.13
Total	99.19	99.95	100.26	101.10	100.97	100.96	99.77	101.16	100.08	101.32
apfu										
$^{X}Na^{+}$	0.66	0.70	0.80	0.82	0.86	0.76	0.69	0.73	0.79	0.78
$^{X}K^{+}$	0.01	0.00	0.00	0.00	0.00	0.00	0.00	0.00	0.00	0.00
$^{X}Ca^{2+}$	0.01	0.01	0.02	0.02	0.02	0.00	0.01	0.00	0.00	0.01
$^{X}\square$	0.32	0.29	0.18	0.16	0.12	0.23	0.30	0.27	0.21	0.21
ΣX	1.00	1.00	1.00	1.00	1.00	1.00	1.00	1.00	1.00	1.00
Li^{+}	0.00	0.33	0.86	0.91	0.91	0.87	0.82	0.88	0.91	0.87
Mg^{2+}	0.05	0.01	0.00	0.00	0.00	0.00	0.00	0.00	0.00	0.00
Fe^{2+}	1.90	1.37	0.44	0.26	0.26	0.17	0.16	0.08	0.07	0.10
Mn^{2+}	0.12	0.15	0.10	0.10	0.09	0.07	0.08	0.07	0.08	0.09
Zn^{2+}	0.12	0.20	0.57	0.68	0.72	0.80	0.81	0.82	0.84	0.88
Al^{3+}	6.79	6.92	7.02	7.05	7.02	7.09	7.12	7.15	7.11	7.06
Ti^{4+}	0.02	0.01	0.00	0.00	0.00	0.00	0.00	0.00	0.00	0.00
$\Sigma(Y+Z)$	9.00	9.00	9.00	9.00	9.00	9.00	9.00	9.00	9.00	9.00
$^{B}B^{3+}$	3.00	3.00	3.00	3.00	3.00	3.00	3.00	3.00	3.00	3.00
$^{T}Si^{4+}$	6.00	6.00	6.00	6.00	6.00	6.00	6.00	6.00	6.00	6.00
O	27.00	27.00	27.00	27.00	27.00	27.00	27.00	27.00	27.00	27.00
$^{V}OH^{-}$	3.00	3.00	3.00	3.00	3.00	3.00	3.00	3.00	3.00	3.00
$^{W}O^{2-}$	0.52	0.33	0.00	0.00	0.00	0.00	0.00	0.00	0.00	0.00
$^{W}OH^{-}$	0.20	0.31	0.40	0.39	0.46	0.67	0.64	0.76	0.78	0.84
$^{W}F^{-}$	0.28	0.36	0.60	0.61	0.54	0.33	0.36	0.24	0.22	0.16
ΣW	1.00	1.00	1.00	1.00	1.00	1.00	1.00	1.00	1.00	1.00
Mn#	0.059	0.099	0.184	0.286	0.252	0.293	0.340	0.439	0.517	0.495
	O-sch	F-sch	F-elb	F-elb	F-elb	Elb	Elb	Elb	Elb	Elb

Mn# = Mn/(Mn+Fe). Abbreviations: O-sch – oxy-schorl, F-sch – fluor-schorl, F-elb – fluor-elbaite, Elb – elbaite.

The content of Zn, generally below 0.20 *apfu* in primary Trm IB, increases up to 6.32 wt.% ZnO (0.76 Zn *apfu*) in Trm IIIA and up to 7.37 wt.% (0.88 Zn *apfu*) in Trm IIIB. Thus, in the absence of Mg, the content of bivalent cations Zn + Fe^{2+} + Mn^{2+} varies from 0.99 to 1.18 *apfu* in Trm IIIA and from 0.93 to 1.15 *apfu* in Trm IIIB, with Zn >> Fe^{2+} > Mn. However, because in all acquired compositions Zn + Fe^{2+} + Mn^{2+} < 1.5 *apfu*, they do not correspond to Zn-dominant tourmaline of hypothetical formula $NaZn_3Al_6B_3Si_6O_{27}(OH)_3(OH)$. The most Zn-enriched compositions yield the formulae:

253 $(Na_{0.73}Ca_{0.01}\square_{0.25})_{\Sigma 1}(Al_{1.03}Li_{0.79}Zn_{0.76}Fe^{2+}_{0.33}Mn_{0.09})_{\Sigma 3}Al_6B_3Si_6O_{27}(OH)_3(F_{0.66}OH_{0.34})$ for Trm IIIA and
254 $(Na_{0.78}Ca_{0.01}\square_{0.21})_{\Sigma 1}(Al_{1.06}Li_{0.87}Zn_{0.88}Fe^{2+}_{0.10}Mn_{0.09})_{\Sigma 3}Al_6B_3Si_6O_{27}(OH)_3(OH_{0.84}F_{0.16})$ for Trm IIIB.
255 The extent of Mn-Fe fractionation also increases from Trm IIIA to Trm IIIB, with Mn/(Mn+Fe)
256 ranging from 0.17 to 0.29 and from 0.29 to 0.52, respectively. However, because Zn fractionates along
257 with Mn, the ratio (Mn+Zn)/(Mn+Zn+Fe+Mg) is a better fractionation index yielding, respectively,
258 0.43–0.74 and 0.81–0.93.

259 *5.5. Compositional relationships*

260 Figure 4 presents variations in concentration of the most important elements in the tourmalines
261 as functions of Mn + Zn fractionation expressed by the ratio (Mn+Zn)/(Mn+Zn+Mg+Fe). Mafic
262 elements, such as Mg, Fe^{2+} and Ti display rather coherent decreasing trends (Figs 4a–c). While
263 present as minor components in Trm IA, Mg and Ti disappear in Trm IB, and may be present only as
264 traces in more fractionated Trm II and Trm III. Iron decreases rapidly from Trm IA to Trm IIB,
265 reaching a relatively constant content of 0.70–0.75 *apfu*. Trm III shows a further steady decrease
266 down to 0.06 Fe *apfu* along with Mn + Zn fractionation. Calcium, a subordinate component in
267 Ti-bearing Trm IA, decreases very rapidly to a trace level in Trm IB (Fig. 4d). However, there is a
268 weak increase in Trm IIA–IIB at the (Mn+Zn)/(Mn+Zn+Mg+Fe) of 0.30–0.40, followed by a regular
269 decrease in more fractionated compositions. Zinc, Mn, ^{Y}Al, Na and F show, at least partly, opposite
270 tendencies (Figs 4e–i) . There is a sharp increase of Mn and Al contents in Trm I owing to Mn-Fe
271 fractionation, as well as dehydroxylation and alkali-vacant substitutions: $Al^{3+} + O^{2-} \rightarrow {}^{Y}(Fe,Mg)^{2+} +$
272 OH^- and $Al^{3+} + \square \rightarrow {}^{Y}(Fe,Mg)^{2+} + {}^{X}Na^+$, respectively. In Zn-poor Trm IIA and IIB both components
273 fluctuate around values of 0.10–0.15 Mn *apfu* and ~1.0–1.3 Al *apfu*. The appearance of Li in
274 tourmaline (from Trm IB to Trm III) changes the compositional relationships between ^{Y}Al and
275 bivalent Y-site cations due to the coupled substitution $Li^+ + Al^{3+} + F^- \rightarrow 2\ {}^{Y}Fe^{2+} + {}^{W}OH^-$ at the Y and W
276 sites. This leads to the crystallization of fluor-elbaite and elbaite (some compositions of Trm II). As a
277 result, Al, Li and Fe^{2+} + Mn + Zn become the only significant Y-site occupants in more fractionated
278 tourmalines. Further compositional evolution is a result of local fluctuation among activities of these
279 components, especially due to dissolution and reprecipitation caused by the (Na,Li,F,B)-enriched
280 fluid, and Mn + Zn *vs*. Fe fractionation.
281 With fractionation, zinc forms a well-defined increasing trend (Fig. 4e), reaching 0.02 *apfu* (0.15
282 wt.% ZnO) in Trm IA, 0.06 *apfu* (0.48 wt.% ZnO) in Trm IB, 0.14 *apfu* (1.17 wt.% ZnO) in Trm IIA, and
283 0.11 *apfu* (0.93 wt.% ZnO) in Trm IIB. Dissolution of gahnite and primary tourmaline and
284 crystallization of secondary Zn-rich Trm III are marked by a sharp increase of Zn content up to 6.32
285 wt.% ZnO (0.76 Zn *apfu*) in Trm IIIA and to 7.37 wt.% (0.88 Zn *apfu*) in Trm IIIB. The stage of
286 atypically high enrichment in Zn in these tourmalines is clearly shown in the
287 (Mn+Zn)/(Mn+Zn+Mg+Fe) *vs*. Mn/(Mn+Fe) plot (Fig. 4j). These two parameters show a simple linear
288 relationship in all tourmaline generations, in which the increasing content of Zn can be attributed
289 only to geochemical fractionation. In the relatively less evolved tourmalines (Trm I–IIB), the
290 maximum values of the two ratios are relatively low, less than 0.30 and 0.20 for
291 (Mn+Zn)/(Mn+Zn+Mg+Fe) and Mn/(Mn+Fe), respectively. In Trm III adjacent to gahnite, Zn
292 suddenly increases, which is marked by the interruption of the trend and a sudden jump of the
293 (Mn+Zn)/(Mn+Zn+Mg+Fe) value to ~0.5–0.7. However, the trend is back to normal at the stage of
294 Trm IIIB crystallization, what suggests the dominance of Mn and Zn fractionation over
295 dissolution–reprecipitation. Such behavior is synchronous with a distinct decrease in F activity,
296 reflected in a gradual transition from the crystallization of fluor-elbaite (Trm IIIA) to elbaite (Trm
297 IIIB) (Fig. 4i).

Preprints (www.preprints.org) | NOT PEER-REVIEWED | Posted: 18 January 2018 doi:10.20944/preprints201801.0176.v1

Peer-reviewed version available at Minerals 2018, 8, 126; doi:10.3390/min8040126

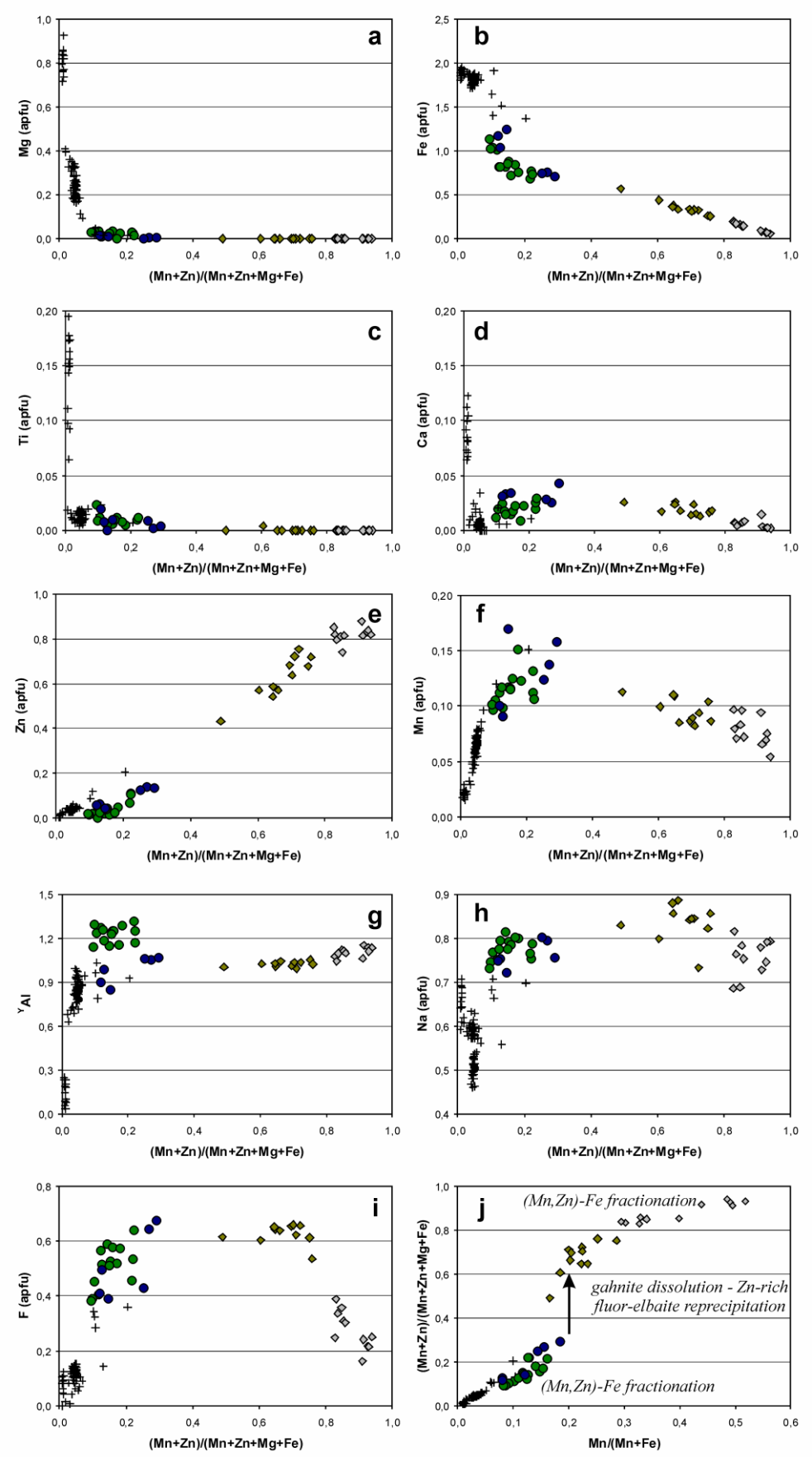

Figure 4. Compositional relationships in tourmalines evolving to Zn-rich fluor-elbaite and elvaite. Symbols: dark crosses – Trm I, dark blue circles – Trm IIA, green circles – Trm IIB, green diamonds – Trm IIIA (Zn-rich fluor-elbaite), grey diamonds – Trm IIIB (Zn-rich elbaite).

5.6. Raman spectroscopy

Figure 5 shows representative unoriented Raman spectra recorded on relicts of primary Li,Al-bearing schorl Trm IB and secondary fluor-elbaite Trm IIIA. Generally, the spectra resemble those for schorl and fluor-elbaite presented by Watenphul et al. ([32]; Fig. 3). In the range of OH stretching vibration modes (3400–3700 cm^{-1}), the spectrum of Zn-rich Trm IIIA has three intense peaks with the maxima at 3498, 3561 and 3596 cm^{-1} (Fig. 5b). Peaks with similar Raman shifts in the spectrum of fluor-elbaite (3494 ± 8, 3562 ± 4 and 3593 ± 4 cm^{-1}) were related by Watenphul et al. [29] to the most probable variants of configurations of the octahedral cations in fluor-elbaite: $^{Y}Li^{Z}Al^{Z}Al$-$2^{Y}Al^{Z}Al^{Z}Al$, $2^{Y}Fe^{*2+Z}Al^{Z}Al$-$^{Y}Al^{Z}Al^{Z}Al$ and $2^{Y}Li^{Z}Al^{Z}Al$-$^{Y}Al^{Z}Al^{Z}Al$, where $^{Y}Fe^{*2+}$ denotes the total of all divalent Y-site occupants ($^{Y}Fe^{*2+}$ = $^{Y}Fe^{2+}$ + $^{Y}Mn^{2+}$ + $^{Y}Zn^{2+}$ + $^{Y}Mg^{2+}$). A visible small asymmetry of the peak 3498 cm^{-1} centered at ~3475 cm^{-1} could come from $^{Y}Fe^{*2+Z}Al^{Z}Al$-$2^{Y}Al^{Z}Al^{Z}Al$ complexes of Y and Z octahedra in the interpretation of Watenphul et al. [32].

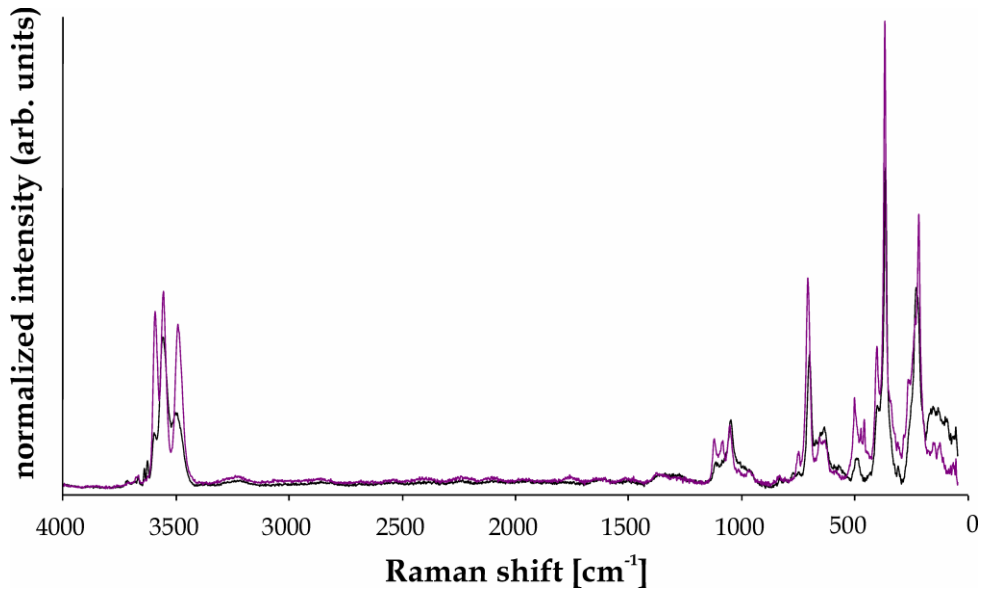

Figure 5. Raman spectra of schorl-type tourmaline Trm IB (black) and Zn-rich fluor-elbaite Trm IIIA (violet) in the range 50–4000 cm^{-1}.

However, we would like to discuss the positions and intensities of the observed bands adopting a slightly different approach. Because ^{V}OH groups occur in the tourmaline structure with an at least 75% abundance relative to the total content of hydroxyls [$3^{V}OH$ + $^{W}(OH,F,O)$], the resulting Raman bands have relatively high intensities. The ^{V}OH groups are bonded to one Y and two Z atoms in the tourmaline structure. Therefore, in all Li-bearing tourmalines only $^{Y}Al^{Z}Al^{Z}Al$, $^{Y}Fe^{*2+Z}Al^{Z}Al$ and $^{Y}Li^{Z}Al^{Z}Al$ arrangements are possible in the YZZ triad around the V=O(3) site. The ^{Z}Al–O(3) and YAl–O(3) bonds are the longest bonds in the Z and Y octahedra, e.g. [33], but the differences with other Z–O or Y–O bonds seems rather too small among various tourmaline species to explain such significant differences in the location of the resulting Raman bands in the spectra of tourmalines. Similarly, this spectral differentiation cannot be explained by different atomic masses of the Y occupants (Li = 6.94, Al = 26.98, Fe = 55.85, Zn = 65.38, …), as the positions of the absorption bands ascribed to different variants of configurations of octahedral cations do not correlate with these data. Therefore, the only plausible explanation is that different positive charges of the Y-occupants (3+, 2+ or 1+), i.e. a charge of atomic nucleolus not compensated by electrons, draw the electron density away from the ^{V}O–H bond, thereby enlarging it but decreasing its strength, in accord with the sequence $^{Y}Al^{3+}$…^{V}O–H (the largest O–H distance; the lowest Raman shift), $^{Y}Fe^{*2+}$…^{V}O–H, and $^{Y}Li^{+}$…^{V}O–H (the shortest O–H distance; the highest Raman shift).

Preprints (www.preprints.org) | NOT PEER-REVIEWED | Posted: 18 January 2018 doi:10.20944/preprints201801.0176.v1

Peer-reviewed version available at Minerals 2018, 8, 126; doi:10.3390/min8040126

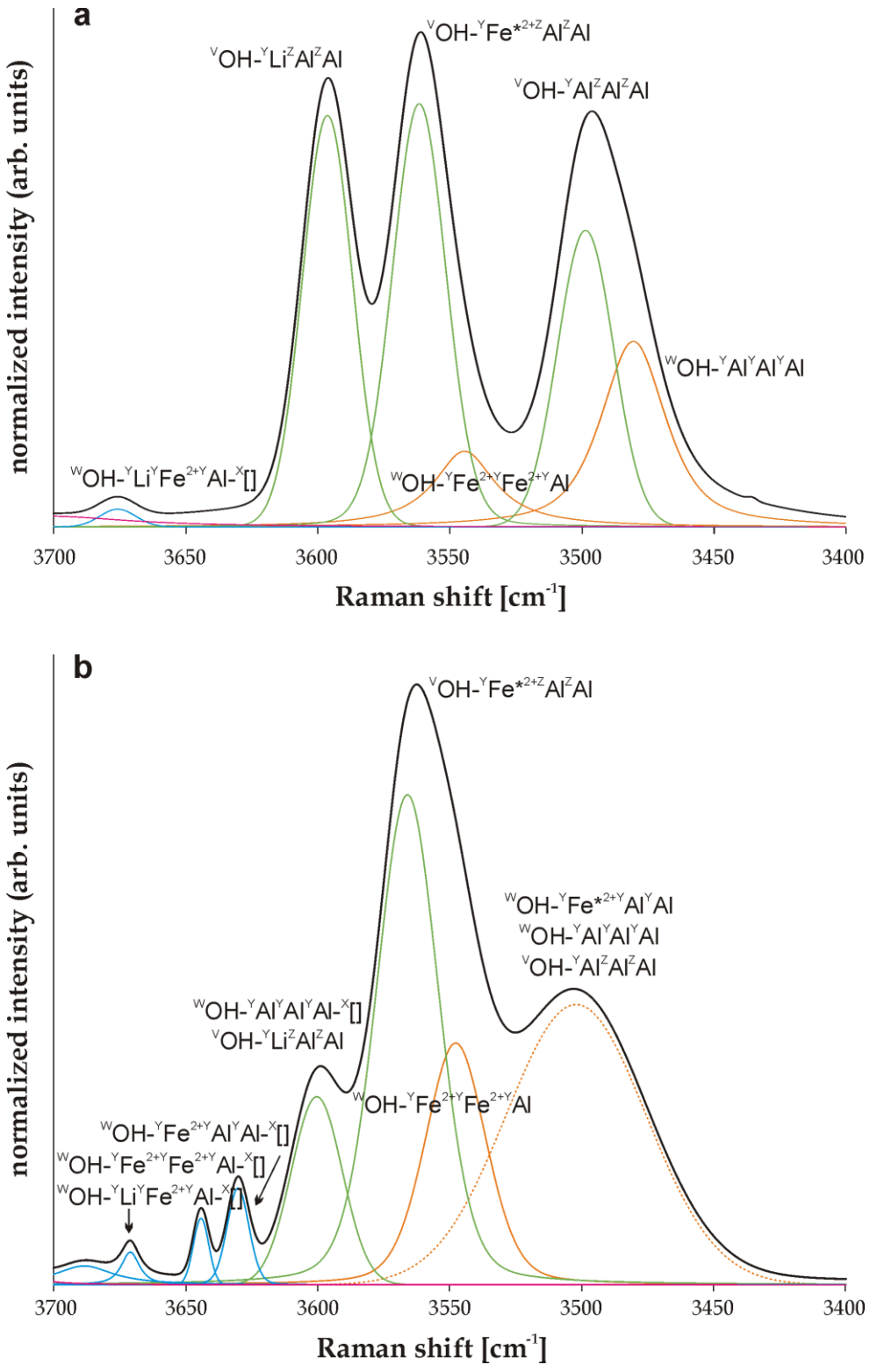

Figure 6. Representative Raman spectra of: (a) primary schorl-type tourmaline (Trm IB) and (b) Zn-rich fluor-elbaite (Trm IIIA) in the range of OH stretching vibrations. Line colours: black – the recorded spectrum, green – bands dominated by ^{V}OH stretching vibrations, orange – bands dominated by ^{W}OH stretching vibrations with Na at the X site (it is not shown in the specifications of the bands), blue – bands dominated by ^{W}OH stretching vibrations with vacancy at the X site, magenta – a baseline. Dotted line marks an unresolved band composed, most likely, from a few significant components.

The ^{W}OH group is bonded to three Y occupants. The presence of Al, Fe^{*2+} and Li at the Y site of the described Zn-rich fluor-elbaite results in 8 allowed models of the YYY triad (LiLiLi and LiLiFe^{*2+} local arrangements are not allowed because local anion bond valence requirements around the W=O(1) site would not be satisfied [34]). It should be expected that, with the small proportion of ^{W}OH in the total OH content (< 25 %), the abundances of individual YYY arrangements would be subordinate and the resulting intensities of the respective stretching vibration bands should be low. Therefore they only have the potential to modify the basic pattern of the spectrum configured essentially by ^{V}OH bands. Applying to the YYY cationic arrangements the same reasoning as the one used above for the YZZ triad, it can be observed that the strongest effect of shifting the electron density away from the ^{W}O–H bond would take place in the ^{Y}Al^{Y}Al^{Y}Al arrangement (associated with the Na-occupied X site), and the weakest for the ^{Y}Li^{Y}Li^{Y}Al and ^{Y}Li^{Y}Fe^{*2+Y}Fe^{*2+} triads. Consequently, the ^{W}O–H bond should be the weakest in case of the first-type triad, and the strongest for the two remaining YYY arrangements. All this considered, the mentioned asymmetry of the 3498 cm^{-1} band observed can be interpreted rather as a result of stretching vibrations with Raman frequency 3480 cm^{-1} in ^{W}OH group bonded to the ^{Y}Al^{Y}Al^{Y}Al arrangement associated with the Na-occupied X site, and not as generated by the arrangement ^{Y}Fe^{*2+Z}Al^{Z}Al-2^{Y}Al^{Z}Al^{Z}Al as was previously assumed [32]. Our interpretation is corroborated by the composition of fluor-elbaite (Trm IIIA), in which the Al content is always slightly higher than the calculated content of Li + Fe^{*2+} (Table 3), which implies the existence of such ^{Y}Al^{Y}Al^{Y}Al sequence. We relate an additional band at 3544 cm^{-1} with a low intensity to vibrations of ^{W}OH group bonded with the ^{Y}Fe^{2+Y}Fe^{2+Y}Al arrangement.

The spectrum of Li,Al-bearing schorl-type tourmaline Trm IB, with three visible maxima in the range of Raman shift below 3600 cm^{-1}, is dominated by 3566 cm^{-1} absorption, interpreted as dominantly coming from stretching vibrations in the ^{V}OH-^{Y}Fe^{*2+Z}Al^{Z}Al arrangement, and a superimposed band 3547 cm^{-1} of lower intensity from ^{W}OH-^{Y}Fe^{*2+Y}Fe^{*2+Y}Al arrangements. The two remaining maxima are related to ^{V}OH-^{Y}Li^{Z}Al^{Z}Al (3601 cm^{-1}) and a relatively wide unresolved band (3502 cm^{-1}), which we interpret as a superposition of ^{V}OH-^{Y}Al^{Z}Al^{Z}Al, ^{W}OH-^{Y}Al^{Y}Al^{Y}Al and ^{W}OH-^{Y}Fe^{*2+Y}Al^{Y}Al bands.

In the case of an absence of Na or Ca at the X site (i.e. the presence of X-site vacancy as e.g. in foitite species), Watenphul et al. [32; Fig. 5] observed a few subordinate bands at wavenumbers generally above 3600 cm^{-1}. They assigned them to stretching vibrations in ^{W}OH groups bonded to YYY triad and associated with unoccupied X site (YYY-^{X}□). Although we generally agree with this interpretation, we propose a slightly different assignment of some individual bands. The X-site vacancy is a result of a common substitution in the tourmaline structure: □ + Me^{3+} → ^{X}Na+ + $^{Y}Me^{2+}$. In this substitution, Me^{3+} cation replaces for Me^{2+} in one octahedron of the Y triad. This means that the only valid YYY cationic arrangements in the structure of various tourmaline species with vacancy at the X site are: ^{Y}Al^{Y}Al^{Y}Al-^{X}□, ^{Y}Fe^{*2+Y}Al^{Y}Al-^{X}□, ^{Y}Fe^{*2+Y}Fe^{*2+Y}Al-^{X}□, ^{Y}Li^{Y}Fe^{*2+Y}Al-^{X}□ and ^{Y}Li^{Y}Al^{Y}Al-^{X}□. As a consequence, weak peaks with Raman shifts at 3630, 3544 and 3671 cm^{-1} in the spectrum of primary schorl-type tourmaline Trm IB can be interpreted as caused by the ^{Y}Fe^{*2+Y}Al^{Y}Al-^{X}□, ^{Y}Fe^{*2+Y}Fe^{*2+Y}Al-^{X}□ and ^{Y}Li^{Y}Fe^{*2+Y}Al-^{X}□ arrangements, respectively, as was proposed by Watenphul et al. [32]. However, the bands are almost invisible in the spectra of Zn-bearing fluor-elbaite Trm IIIA, although the EMPA data suggest that X site in this tourmaline is similarly not fully occupied (Table 3). We interpret it as an indication that ^{X}□ is essentially connected with ^{Y}Al^{Y}Al^{Y}Al triad as a result of the aforementioned substitution in the primary ^{Y}Fe^{*2+Y}Al^{Y}Al triad. The ^{Y}Al^{Y}Al^{Y}Al cationic arrangement shows the strongest effect of shifting the electron density away from the ^{W}O–H bond and is characterized by the strongest increase of the ^{W}O–H distance that weakens the ^{W}O–H bond. As a consequence, the resulting band should be located at a lower wavenumber in the spectrum compared to other valid YYY-^{X}□ arrangements. In our opinion, the absorption band related to the ^{W}OH-^{Y}Al^{Y}Al^{Y}Al-^{X}□ arrangement is superimposed on the much more intensive ^{V}OH-^{Y}Li^{Z}Al^{Z}Al band and therefore is not discernible in the spectra of both tourmalines. The band at 3676 cm^{-1} related to ^{Y}Li^{Y}Fe^{*2+Y}Al-^{X}□ arrangements is the only of this group to appear in the spectrum of Zn-rich fluor-elbaite Trm IIIA. It can easily be explained as the three cations are the main Y-constituents in this tourmaline.

4. Discussion: is natural Zn-dominant tourmaline possible?

The Zn-rich tourmaline (Trm III) from the Julianna system of anatectic pegmatites at Piława Górna is fluor-elbaite and elbaite with a composition close to $Na(LiAlZn)Al_6B_3Si_6O_{27}(OH)_3F$, where Zn can be partly replaced by Fe^{2+} and Mn^{2+} (Zn >> Fe > Mn). Sokolov et al. [15], described a Zn-bearing tourmaline with a Zn content about half that from Piława Górna, and suggested the possible end-member composition $NaZn_3Al_6B_3Si_6O_{27}(OH)_3(OH)$ for a hypothetical Zn-tourmaline. However, two other hypothetical end-members are also possible: $\square(Zn_2Al)Al_6B_3Si_6O_{27}(OH)_3(OH)$ and $Na(Zn_2Al)Al_6B_3Si_6O_{27}(OH)_3O$. In order to discuss the possibility of the existence of natural Zn-tourmaline two issues should be considered: (1) whether Zn alone or Zn + 0.5Al could dominate the Y site, and (2) which anion might be expected to be dominant at the W site of this tourmaline.

Zinc is only a very subordinate incompatible component of silicate magmas, and its lithophile affinity is restricted by the presence of sulphide species. Geochemical fractionation leads to the enrichment of granitic melts, particularly peralkaline magmas, in Zn and favours crystallization of gahnite as a minor accessory mineral in peraluminous leucogranites, pegmatitic granites and granitic pegmatites, as well as incorporation of traces of Zn into crystal structures of some primary phosphates, e.g. triphylite, lithiophilite, sarcopside or graftonite-group minerals [35]. Lithophile behaviour of Zn in the Piława Górna pegmatitic system is evidenced by the crystallization of accessory Zn-bearing ilmenite-pyrophanite and gahnite in moderately fractionated dykes, and the assemblage of gahnite, Zn-bearing ferronigerite and zinconigerite, as well as genthelvine and Zn-bearing helvine in highly-fractionated ones.

In tourmaline-supergroup minerals, Zn is an accessory component commonly occurring in amounts up to a few tenths of ZnO wt.%. Such low concentrations indicate that Zn only slightly fractionates versus Fe in the tourmaline structure. In the Piława Górna pegmatites, even tourmalines from highly-fractionated dykes only occasionally have more than 1 wt.% ZnO. This fact suggests that hypothetical Zn-dominant tourmaline will rather not form due to Zn-Fe fractionation even in geochemically highly-evolved environments. Thus, it seems that the only specific mechanism that can promote crystallization of Zn-rich tourmaline is Na-Li-B-F metasomatism of a gahnite-bearing mineral assemblage. The Zn-rich fluor-elbaite + elbaite (Trm III) from Piława Górna are an example, where the local crystallization environment was controlled by dissolution of gahnite by aggressive (Na,Li,F,B)-bearing fluids. Crystallization of Zn-rich tourmaline was, however, limited to a relatively narrow 0.1-millimetre-sized zone around gahnite, which suggests low diffusion of Zn toward fluor-elbaite overgrowths. Therefore, single crystals of Zn-dominant tourmaline seem rather unlikely in nature and intergrowths of gahnite with Li-bearing tourmalines (Na-Li-B-F metasomatism around gahnite) might be the most favourable environment where zones/domains of Zn-dominant tourmaline could form.

All known tourmalines with elevated Zn contents are elbaite or fluor-elbaite [9–15; present study]. The excesses of Al over Li and high amounts of X-site vacancies or $^{W}O^{2-}$ could favour the formation of Zn-tourmaline with dominance of the end-members $\square(Zn_2Al)Al_6B_3Si_6O_{27}(OH)_3(OH)$ or $Na(Zn_2Al)Al_6B_3Si_6O_{27}(OH)_3O$. However, Zn-rich fluor-elbaite with the presence of significant X-site vacancies or $^{W}O^{2-}$ could also be interpreted as a solid solution of $NaZn_3Al_6B_3Si_6O_{27}(OH)_3(OH)$ tourmaline with fluor-elbaite + rossmanite or darrelhenryite end-members, as such a case is rather shown by Raman spectra of Zn-rich fluor-elbaite Trm III. This implies that fluorine, as a significant component of the Zn-rich tourmalines, should be intimately related to the fluor-elbaite constituent, and the W site in Zn-dominant tourmaline should rather be dominated by OH or O.

5. Conclusions

Atypically high Zn enrichment in tourmaline is generally connected with certain elbaites and fluor-elbaites. The enrichment in Zn does not result from Zn-Fe fractionation, but rather from dissolution of gahnite by (Na,Li,F,B,Be)-bearing fluid and reprecipitation of Zn-bearing secondary fluor-elbaite or elbaite in the nearest neighborhood of the decomposing gahnite. As fluorine is incorporated into tourmaline by the fluor-elbaite component, three potential Zn-dominant end-members for Zn-tourmaline are possible: $NaZn_3Al_6B_3Si_6O_{27}(OH)_3(OH)$,

□(Zn$_2$Al)Al$_6$B$_3$Si$_6$O$_{27}$(OH)$_3$(OH) and Na(Zn$_2$Al)Al$_6$B$_3$Si$_6$O$_{27}$(OH)$_3$O. Future structural studies are needed to determine which of the hypothetical end-members is more likely.

Acknowledgments: We thank … for their comments on this manuscript. The studies were supported by the National Science Centre (Poland) grant 2015/19/B/ST10/01809 to AP.

Author Contributions: A.P. designed the scientific topic of the work, made all compositional recalculations and wrote the paper; A.W. and E.S. performed the EMP analysis; B.G and P.J. recorded and resolved Raman spectra of the tourmalines; and A.Sz. edited text of the manuscript and prepared graphs.

Conflicts of Interest: The authors declare no conflict of interest. The founding sponsors had no role in the design of the study; in the collection, analyses, or interpretation of data; in the writing of the manuscript, and in the decision to publish the results.

References

1. Henry, D.J.; Novák, M.; Hawthorne, F.C.; Ertl, A.; Dutrow, B.L.; Uher, P.; Pezzotta, F. Nomenclature of the tourmaline-supergroup minerals. *Am. Mineral.* **2011**, *96*, 895–913, DOI: 10.2138/am.2011.3636.
2. Sokolov, M.; Martin, R.F. A Pb-dominant member of the tourmaline group, Minh Tien granitic pegmatite, Luc Yen District, Vietnam. *Estudos Geológicos* **2009**, *19*, 352–353.
3. Lottermoser, B.G.; Plimer, I.R. Chemical variation in tourmalines, Umberatana, South Australia. *N. Jb. Miner. Mh.* **1987**, *7*, 314–326.
4. Yu, J.M.; Jiang, S.Y. Chemical composition of tourmaline from the Yunlong tin deposit, Yunnan, China: implications for ore genesis and mineral exploration. *Miner. Petrol.* **2003**, *77*, 67–84, DOI: 10.1007/s00710-002-0195-2.
5. Johnson, M.L.; Wentzell, Ch.Y.; Elen, S. Multicolored bismuth-bearing tourmaline from Lundazi, Zambia. *Gems & Gemology* **1997**, *33*, 204–211, DOI: 10.5741/GEMS.33.3.204.
6. Vereshchagin, O.S.; Rozhdestvenskaya, I.V.; Frank-Kamenetskaya, O.V.; Zolotarev, A.A.; Mashkovtsev, R.I. Crystal chemistry of Cu-bearing tourmalines. *Am. Mineral.* **2013**, *98*, 1610–1616., DOI: 10.2138/am.2013.4408.
7. Baksheev, I.A.; Kudryavtseva, O.E. Nickeloan tourmaline from the Berezovskoe gold deposit, Middle Urals, Russia. *Can. Mineral.* **2004**, *42*, 1065–1078, DOI: 10.2113/gscanmin.42.4.1065.
8. Grice, J.D.; Ercit, T.S. Ordering of Fe and Mg in the tourmaline crystal structure: The correct formula. N. Jb. *Miner. Abh.* **1993**, *165*, 245–266.
9. Federico, M.; Andreozzi, G.B.; Lucchesi, S.; Graziani, G. Compositional variation of tourmaline in the granitic pegmatite dykes of the Cruzeiro Mine, Minas Gerais, Brazil. *Can. Mineral.* **1998**, 36, 415–431.
10. Hawkins, K.D.; MacKinnon, I.D.R.; Schneeberger, H. Influence of chemistry on the pyroelectric effect in tourmaline. *Am. Mineral*. **1995**, *80*, 491–501, DOI: 10.2138/am-1995-5-610.
11. Jedwab, J. Tourmaline zincifere dans une pegmatite de Muika (Congo). Bulletin de la Société belge de géologie, de paléontologie et d'hydrologie **1962**, *71*, 132–135.
12. Adusumilli, M.S.; Castro, C.; Bhaskara Rao, A. Blue and green gem tourmalines from Gregório pegmatite, Rio Grande do Norte State, Brazil. In 16th General Meeting, IMA. Pisa, Italy, 1994, pp. 1–13.
13. Soares, D.R. Contribuição à petrologia de pegmatitos mineralizados em elementos raros e em elbeítas gemológicas da Província Pegmatítica da Borborema, Nordeste do Brasil. Ph.D. thesis. UFPE, Recife, Brazil, 2004.
14. Ferreira, A.C.M.; Ferreira, V.P.; Soares, D.R.; Vilarroel-Leo, H.S. Chemical and mineralogical characterization of elbaite from the Alto Quixaba pegmatite, Seridó Province, NE Brazil. *An. Acad. Brasil. Ciências* **2005**, *77*, 729–743.
15. Sokolov, P.B.; Gorskaya, M.G.; Kretser, Yu.L. Zinc-bearing tourmalines from rare-metal pegmatites. *Zap. Vses. Mineral. Obshchest.* **1988**, *117*, 70–74. (in Russian).
16. Szuszkiewicz, A.; Szełęg, E.; Pieczka, A.; Ilnicki, S.; Nejbert, K.; Turniak, K.; Banach, M.; Łodziński, M.; Różniak, R.; Michałowski, P. The Julianna pegmatite vein system at the Piława Górna mine, Góry Sowie Block, SW Poland – preliminary data on geology and descriptive mineralogy. *Geol. Quart.* **2013**, *57*, 467–484, DOI: 10.7306/gq.1097.
17. Pieczka, A.; Łodziński, M.; Szełęg, E.; Ilnicki, S.; Nejbert, K.; Szuszkiewicz, A.; Turniak, K.; Banach, M.; Michałowski, P.; Różniak, R. The Sowie Mts. pegmatites (Lower Silesia, SW Poland): a current knowledge. *Acta Mineral.-Petrogr., Szeged* **2012**, *7*, 105–106.

18. Pieczka, A.; Szuszkiewicz, A.; Szełęg, E.; Nejbert, K.; Łodziński, M.; Ilnicki, S.; Turniak, K.; Banach, M.; Hołub, W.; Michałowski, P.; Różniak, R. (Fe,Mn)–(Ti,Sn)–(Nb,Ta) oxide assemblage in a little fractionated portion of a mixed (NYF + LCT) pegmatite from Piława Górna, the Sowie Mts. block, SW Poland. *J. Geosci.* **2013**, *58*, 91–112, DOI: 10.3190/jgeosci.136.
19. Pieczka, A.; Szuszkiewicz, A.; Szełęg, E.; Janeczek, J.; Nejbert, K. Granitic pegmatites of the Polish part of the Sudetes (NE Bohemian massif, SW Poland). In Fieldtrip Guidebook, 7th International Symposium on Granitic Pegmatites, PEG 2015 , Książ, Poland, June 17–19 2015, Gadas P., Novák M., Szuszkiewicz A., Cempírek J., Eds.; Czech Republic, 2015, pp. 73–103.
20. Pieczka, A.; Szuszkiewicz, A.; Szełęg, E.; Ilnicki, S.; Nejbert, K.; Turniak, K. Samarskite-group minerals and alteration products: an example from the Julianna pegmatitic system, Piława Górna, SW Poland. *Can. Mineral.* **2014**, *52*, 303–319, DOI: 10.3749/canmin.52.2.303.
21. Pieczka, A.; Szełęg, E.; Szuszkiewicz, A.; Gołębiowska, B.; Zelek, S.; Ilnicki, S.; Nejbert, K.; Turniak, K. Cs-bearing beryl evolving to pezzottaite from the Julianna pegmatitic system, SW Poland. *Can. Mineral.* **2016**, *54*, 115–124, DOI: 10.3749/canmin.1500075.
22. Szuszkiewicz, A.; Pieczka, A.; Szełęg, E.; Turniak, K.; Ilnicki, S.; Nejbert, K. The euxenite-group minerals and products of their alteration in the hybrid Julianna granitic pegmatite, Piława Górna, Sudetes, southwestern Poland. *Can. Mineral.* **2016**, *54*, 4, 879–898, DOI: 10.3749/canmin.1600023.
23. Pieczka, A.; Hawthorne, F.C.; Cooper, M.A.; Szełęg, E.; Szuszkiewicz, A.; Turniak, K.; Nejbert, K.; Ilnicki, S. Pilawite-(Y), $Ca_2(Y,Yb)_2[Al_4(SiO_4)_4O_2(OH)_2]$, a new mineral from the Piława Górna granitic pegmatite, southwestern Poland: mineralogical data, crystal structure and association. *Min. Mag.* **2015**, *79*, 1143–1157, DOI: 10.1180/minmag.2015.079.5.09.
24. Szełęg, E.; Zuzens, B.; Hawthorne, F.C.; Pieczka, A.; Szuszkiewicz, A.; Turniak, K.; Nejbert, K.; Ilnicki, S.S.; Friis, H.; Makovicky, E.; Weller, M.T.; Lemèe-Cailleau, M.-H. Bohseite, ideally $Ca_4Be_4Si_9O_{24}(OH)_4$, from the Piława Górna quarry, the Góry Sowie Block, SW Poland. *Min. Mag.* **2017**, *81*, 35–46, DOI: 10.1180/minmag.2016.080.
25. Pieczka, A.; Hawthorne, F.C.; Ma, C.; Rossman, G.; Szełęg, E.; Szuszkiewicz, A.; Turniak, K.; Nejbert, K.; Ilnicki, S.S. Żabińskiite, ideally $Ca(Al_{0.5}Ta_{0.5})(SiO_4)O$, a new mineral of the titanite group from the Piława Górna pegmatite, the Góry Sowie Block, southwestern Poland. *Min. Mag.* **2017**, *81*, 591–610, DOI: 10.1180/minmag.2016.080.110.
26. Turniak, K.; Pieczka, A.; Kennedy, A.K.; Szełęg, E.; Ilnicki, S.; Nejbert, K.; Szuszkiewicz, A. Crystallisation age of the Julianna pegmatite system (Góry Sowie Block, NE margin of the Bohemian massif): evidence from U–Th–Pb SHRIMP monazite and CHIME uraninite studies. In Fieldtrip Guidebook, 7th International Symposium on Granitic Pegmatites, PEG 2015 , Książ, Poland, June 17–19 2015, Gadas P., Novák M., Szuszkiewicz A., Cempírek J., Eds.; Czech Republic, 2015, 111–112.
27. Van Breemen, O.; Bowes, D.R.; Aftalion, M.; Żelaźniewicz, A. Devonian tectonothermal activity in the Sowie Góry gneissic block, Sudetes, southwestern Poland: evidence from Rb–Sr and U–Pb isotopic studies. *Ann. Geol. Soc. Pol.* **1988**, *58*, 3–10.
28. Timmermann, H.; Parrish, R.R.; Noble, S.R.; Kryza, R. New U–Pb monazite and zircon data from the Sudetes Mountains in SW Poland:, evidence for a single-cycle Variscan orogeny. *J. Geol. Soc.* **2000**, *157*, 265–268, DOI: 10.1144/jgs.157.2.265.
29. Kryza, R.; Fanning, C.M. Devonian deep-crustal metamorphism and exhumation in the Variscan Orogen: evidence from SHRIMP zircon ages from the HT–HP granulites and migmatites of the Góry Sowie (Polish Sudetes). *Geodinamica Acta* **2007**, *20*, 159–176, DOI: 10.3166/ga.20.159-175.
30. Müller, A.; Szuszkiewicz, A.; Ilnicki, S.; Nejbert, K. Quartz chemistry of the Julianna pegmatites and their wall rocks, Piława Górna, Poland: implications for the origin of pegmatite melts. In Abstracts and Proceedings of the 8th International Symposium on Granitic Pegmatites, PEG2017, 13th–15th June 2017, Kristiansand, Norway. Müller, A., Rosing-Schow, N. Eds., Norsk Geologisk Forening, Trondheim, Norway, pp. 84–88.
31. Pouchou, I. L.; Pichoir, F. "PAP" (phi-rho-z) procedure for improved quantitative microanalysis. In *Microbeam Analysis*, Armstrong, I.T.; Ed., San Francisco Press, San Francisco. 1985, pp. 104–106.
32. Watenphul, A.; Burgdorf, M.; Schlüter, J.; Horn, I.; Malcherek, T.; Mihailova, B. Exploring the potential of Raman spectroscopy for crystallochemical analyses of complex hydrous silicates: II. Tourmalines. *Am. Mineral.* **2016**, *101*, 970–985, DOI: 10.2138/am-2016-5530.

33. Choi, J.B., Hawthorne, F.C. Characterization of tourmaline crystals by Rietveld and single-crystal structure refinement: A comparative study. *Geosci. J.* **2002**, *6*, 237–243.
34. Hawthorne, F.C. Structural mechanism for light-element variations in tourmaline. *Can. Mineral.* **1996**, *34*, 123–132.
35. Černý, P.; Meintzer, R.E.; Anderson, A.J. Extreme fractionation in rare-element granitic pegmatites: selected examples of data and mechanism. *Can. Mineral.* **1985**, *23*, 381–421.